PCCP

ROYAL SOCIETY OF CHEMISTRY

PAPER

Cite this: *Phys. Chem. Chem. Phys.*, 2022, **24**, 21822

Formation of the quasi-planar B_{56} boron cluster: topological path from B_{12} and disk aromaticity†

Fernando Buendía,[a] Hung Tan Pham,[b] José Enrique Barquera-Lozada,[c] Marcela R. Beltrán Sanchez[d] and Minh Tho Nguyen[*e]

Received 6th June 2022,
Accepted 26th August 2022

DOI: 10.1039/d2cp02571j

rsc.li/pccp

Formation and stability of the B_{56} boron cluster were investigated using a topological approach and the disk aromaticity model. An extensive global energy minimum search for the B_{56} system which was carried out by means of the Mexican Enhanced Genetic Algorithm (MEGA) in conjunction with density functional theory computations, confirms a quasi-planar structure as its energetically most stable isomer. Such a structural motif is derived by applying a topological leapfrog operation to a B_{12} form. Its high thermodynamic stability can be explained by the disk aromaticity model in which the delocalization of its π orbitals can be assigned to the levels of a particle in a circular box with the $[(1\sigma)^2\ (1\pi)^4\ (1\delta)^4\ (1\varphi)^4\ (2\sigma)^2\ (1\gamma)^4\ (2\pi)^4\ (2\delta)^4\ (1\eta)^4\ (2\varphi)^4\ (1\theta)^2]$ electronic configuration. This π delocalization is confirmed by other delocalization indices. While the B_{56} has a similar electron delocalization to that of the quasi-planar B_{50}, they have opposite magnetic ring current properties because of the symmetry selection rules of their HOMO–LUMO electronic transitions. The π delocalization in the boron clusters is larger at long distances as compared to carbon clusters at similar sizes, but such a trend is reversed at shorter distances.

1. Introduction

The boron clusters form a rich and colorful family of nanoclusters owing to the great diversity of their structural motifs, electronic features and chemical bonding phenomena.[1–3] Structures of the pure boron clusters B_n include the planar and quasi-planar forms, bowl, tube, ribbon, cage, double layer, fullerene, bucky-ball,... whose electronic structure and bonding do not always follow the conventional rules and models.[4–7] Different models have therefore been introduced to rationalize their diverging characteristics. The aromaticity remains one of the most popular models for characterizing planar compounds. While the structures of small-sized planar and quasi-planar boron clusters[4,8–11] can be accounted for by the classical Hückel rule for aromaticity, those of the larger planar and quasi-planar species having a circular shape do not obey the $4N + 2$ electron count but can be understood through the disk aromaticity model,[2,12–14] which provides us with an effective interplay between the shape of some planar or quasi-planar clusters and their high stability. For example, the disk aromaticity was demonstrated to be the main contributor to the thermodynamic stability of the planar B_{18}^{2-}, B_{19}^{-}, B_{20}^{2-}, and B_{50} clusters,[13–15] as well as the bowl-shaped B_{30}, B_{36} and B_{42} structures.[16] Other aromaticity models have also been proposed to explain the aromaticity character of the planar elongated ribbon,[17,18] or rectangular[19,20] structures.

Concerning the stability and growth pattern of the pure B_n boron clusters, the current intensive studies point out that they still are a mystery. Indeed, a planar or quasi-planar shape is favored for the sizes up to $n = 16$ for cations, $n = 19$ for neutrals and up to $n = 27$ for anion.[15,21,22] However, the neutral B_{14} fullerene emerges as an exception of the planar shape tendency.[23] Starting from the size of B_{20}, a double ring tube connecting two B_n strings in an anti-prism manner is found as the ground state of B_{20}, B_{22}, B_{24} and B_{26} clusters in the neutral state.[1] More particularly, B_{27}^{+} and B_{42} exhibit each a triple ring tubular shape in which their geometry is constructed by superposing three B_9 and B_{14} strings in anti-prism fashion, respectively.[1,24] These sizes show that a tubular shape is also an inherent structural motif of boron clusters beside the planar one. The hollow cylinder model (HCM)[7,25] has been proved to be more suitable for rationalizing the aromaticity in tubular shape. In growing further, both B_{28} and B_{29} turn out to have a

[a] *Instituto de Física, Universidad Nacional Autónoma de México, C.P. 04510 Cd. de México, Mexico*
[b] *Department of Chemistry, KU Leuven, Celestijnenlaan 200F, B-3001 Leuven, Belgium*
[c] *Instituto de Química, Universidad Nacional Autónoma de México, C.P. 04510 Cd de México, Mexico*
[d] *Instituto de Investigaciones en Materiales, Universidad Nacional Autónoma de México, C.P. 04510 Cd. de México, Mexico*
[e] *Institute for Computational Science and Technology (ICST), Ho Chi Minh City, Vietnam. E-mail: tho.nm@icst.org.vn*

† Electronic supplementary information (ESI) available: Table lists the Cartesian coordinates of the optimized geometries of the isomers A–J. See DOI: https://doi.org/10.1039/d2cp02571j

cage-like structure rather than a planar or tubular shape emphasizing the unpredictability of boron cluster structures.[1,3,7,24]

Then the appearance of bowl-shaped boron clusters brought in a surprise. Numerous studies demonstrated that the B_{26}^-, B_{30}, B_{32}, B_{33}^-, B_{34}^-, $B_{35}^{-/0}$, and B_{36} clusters are, among others, classified into a bowl-like class which contains either one pentagonal or one hexagonal hole.[7,12,26,27] B_{32} was however shown to have a more stable double ring of two 16-strings.[28] The following sizes B_{37}^- and B_{38}^- also exhibit bowl-shaped structures but with two hexagonal holes.[17] The appearance of several bowl-shaped structures led to an assumption that these small size boron clusters could be part of the boron sheets, and some kinds of planar structure were predicted to be favored for subsequent sizes. However, a number of cage-like or fullerene structures have been found as the global energy minimum isomers for the larger sizes including B_{39}^+, B_{40}, B_{41}^+, B_{42}^+, B_{44}, and B_{46}.[7,19,29] The B_{46} was predicted to be a cage with an octagonal hole, but subsequent calculations showed that a core–shell structure with four internal B atoms could be more stable, in such a way that the global minimum of B_{46} is not well established yet. A double layer structural pattern was suggested for B_n with n from 48 to 72 atoms.[30–32] Such a structure has been corroborated with some experimental results in the case of B_{48}^-.[33] The emergence of fullerene-like, core–shell and double-layer seems to suggest that the behavior of boron clusters could be similar to that of the isovalent aluminum clusters at larger sizes.[34–36] Contrary to such an expectation, a quasi-planar structure shown in Fig. 1 containing two hexagonal holes was found as the lowest-energy isomer for the B_{50} size.[14]

We demonstrated that the shape of the quasi-planar B_{50} displayed in Fig. 1 is actually produced from the topological leapfrog principle.[14] Starting from a B_{10}^{2-} geometry which is the smallest elongated boron cluster, application of the leapfrog principle excellently reproduces a B_{50} planar shape (Fig. 1). Perhaps more importantly, the high thermodynamic stability of B_{50} can be rationalized in terms of the disk aromaticity model. More recently the shape of a planar B_{24} cluster can also be reproduced by applying the leapfrog operation, even it is not the lowest-lying isomer, being less stable than the double ring of two B_{12} strings. Overall, it appears that the geometry of a boron cluster can be predicted from that of a smaller size, at least for the planar forms. Concerning the following B_{56} size, Li *et al.*[31] suggested, using density functional theory computations, a quasi-planar B_{56} structure (**A**) as displayed in Fig. 1 which contains two hexagonal holes as its global energy minimum, on the basis of six lowest-lying isomeric candidates. This finding illustrates once more that the growth pattern of the pure boron clusters is far from regular and not fully understood yet. In this context, we set out to carefully identify the global minimum structure of the B_{56} cluster in carrying out. One the one hand an extensive search using a genetic algorithm developed by us, and on the other hand a topological analyze of its geometrical shape using the leapfrog principle which was successful for predicting the B_{50} structure. Subsequently, its electronic structure and bonding pattern are analysed and its aromatic character is probed using the magnetic ring current computations. Let us mention that the stability and electronic properties of B_{40} and B_{50} clusters are of current interest for applications as sensors of different pollutant gases.[37,38]

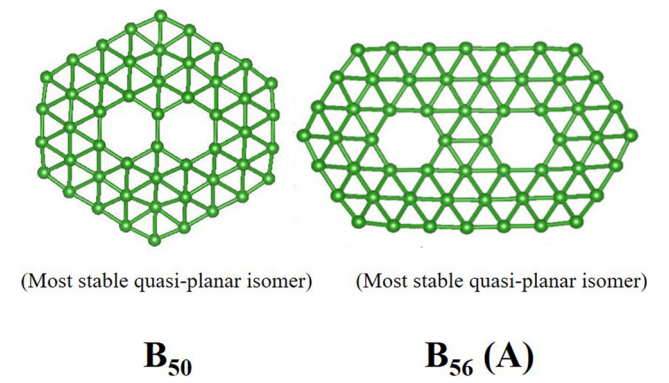

Fig. 1 Shapes of the most stable B_{50} and B_{56} boron clusters.

2. Methods and results

2.1 The global energy minimum structure of B_{56}

The energetically most stable isomer of the B_{56} cluster has been reported before,[31] but it is of crucial importance to confirm its identity. In order to find this isomer, we use a genetic algorithm code, the Mexican Enhanced Genetic Algorithm (MEGA),[39] which is implemented within the Vienna *ab initio* simulation package (VASP).[40–43] Let us briefly mention the main operations. Geometry optimizations utilize the PBE exchange and correlation functional[44] which is known to provide good results for boron clusters[14,45] and a plane-wave basis set with an energy cut-off of 400 eV. In this search, the initial population (pool) consists of structures which are randomly generated or suggested from earlier studies. Once an initial pool has been reached, the MEGA algorithm applies mate or mutation operations on the pool structures to generate new structures and subsequently optimizes them using the VASP program to selectively sample the complex potential energy surface. Details of these operations have been described in a previous work.[39] For B_{56}, the mutations called "move" (a slight random displacement of atoms) and "rotate" (rotation of a few atoms with respect to the rest around a random axis) are employed. The new geometries generated consist of 80% by the mate operator and 20% by the mutation operators.

The search for energy minimum using the MEGA genetic algorithm is carried out with five different initial pools. While the first pool is generated from scratch, the other four pools are constructed on the basis of previous results of elemental clusters having the same and smaller sizes. The search of the lowest energy isomer for B_{56} includes about seven thousands different geometries using five initial pools.

Due to the use of plane-wave basis set which is not a perfect approach for gas phase clusters, the structures obtained from the MEGA search are subsequently re-optimized using the hybrid TPSSh functional in conjunction with the 6-311+G(d)

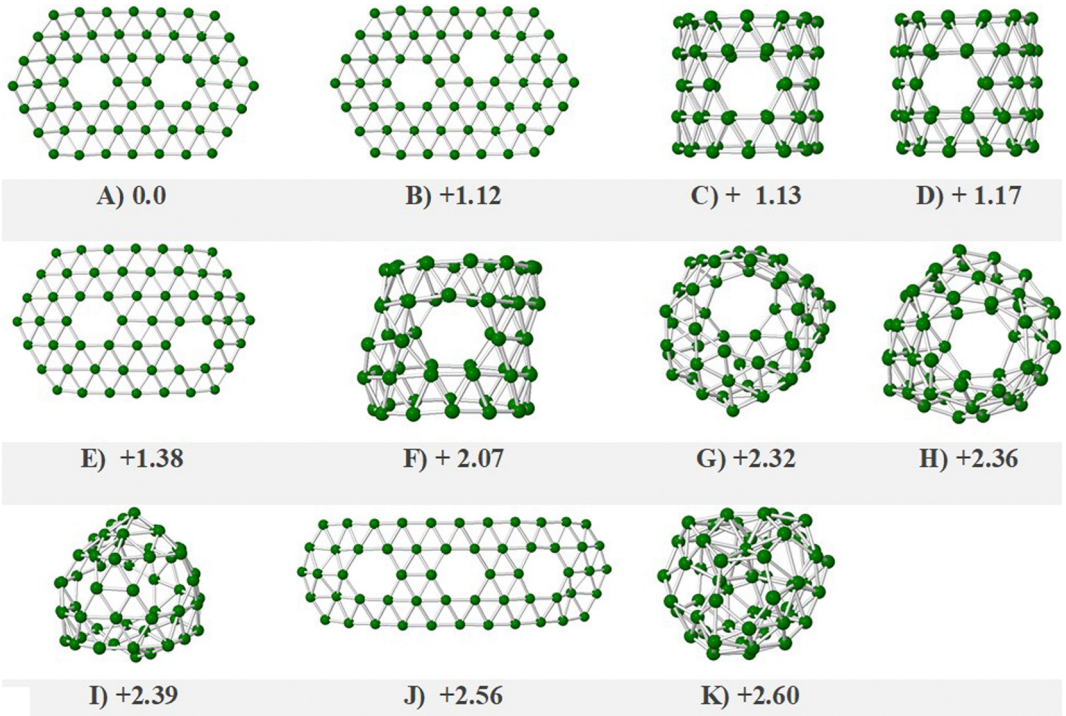

Fig. 2 Geometric shapes of the lowest-lying B_{56} isomers obtained from geometry optimizations performed using TPSSh/6-311+G(d). Relative energies are presented in eV with ZPE corrections.

basis set, followed by an analysis of their harmonic vibrational frequencies at the same level. The identity of the isomers remains unchanged upon re-optimization. Fig. 2 displays some low-lying B_{56} isomers. Accordingly, the isomer **A** (Fig. 1) is identified as the lowest energy structure confirming a previous report.[32] It is clear that isomer **A** exhibits a quasi-planar form with two hexagonal holes.

In order to further check the identity of the B_{56} lowest-lying isomer, we carry out additional genetic searches. First, we perform two sets of search beginning from scratch, and we find some good candidates closed in energy to the lowest-energy isomer as a pentagonal ring with four non-symmetrical holes **C**. This structure is however the third lowest-energy isomer and at 26 kcal mol^{-1} (1.1 eV) higher in energy. Another three systems **G**, **H** and **I** without symmetry and with cage-like structures are also found and shown in Fig. 2. These structures are computed to be 53, 54, and 55 kcal mol^{-1} (2.3, 2.4 and 2.4 eV) higher in energy, respectively. Each of these structures possesses at least two hexagonal holes; such a feature is likely due to the electron deficiency of the boron atom.

For the search that begins using structures containing ring structures as initial pool, we employ tri-, tetra- and penta-holes that have been located as the lowest-energy isomers for smaller systems, and also the pentagonal rings with four hexagonal non-symmetrical holes. The MEGA genetic algorithm search locates only one new geometry that is closer in energy than the previous results of the search beginning from scratch. This is, the pentagonal ring with four non-symmetrical holes **D** and 27 kcal mol^{-1} (1.2 eV) higher in energy than the lowest-energy isomer **A**, and the symmetry of this geometry is reduced to a C_2 point group. Some isomers having tetragonal ring structures are also found but they are associated with low stability.

Another initial pool employed with the MEGA algorithm is composed by core–shell structures such as in the B_{46} size which was claimed as its lowest-energy isomer.[38] The structures obtained within this series are not as stable as those of the other family of candidates; the lowest isomer **K** of this pool lies at 60 kcal mol^{-1} (2.6 eV) higher in energy (Fig. 2), and this structure has 3 boron atoms forming a triangular central core.

Finally, the initial pool of the last search consists in some quasi-planar structures that have been found as the lowest energy isomers for smaller boron clusters as B_{36}, B_{40}, B_{50} and other good candidates obtained previously. From this search, the lowest energy isomer **A** is again confirmed. The two other structures **B** and **E** are higher in energy by 26 and 32 kcal mol^{-1} (1.1 and 1.4 eV), respectively. Both have similar shape, but the two hexagonal holes in each structure are located at different positions. The last quasi-planar structure **J** (Fig. 2) with three holes but with one side larger than the lowest energy isomer and with a bigger curvature is 59 kcal mol^{-1} (2.6 eV) higher in energy.

2.2 A topological path from B_{12} leading to formation of B_{56}

In an attempt to understand where the quasi-planar structure **A** comes from, we now apply a topological leapfrog process which has successfully generated the stable isomers for carbon clusters and boron cages.[3,46] In the case of the carbon fullerenes,[46] the leapfrog process includes the omni-capping and dual operations whereas for the boron systems, an additional boron cap must be applied due to the electron deficit of the boron atom.[14,20]

As stated above, the shape of the most stable quasi-planar B_{50} structure was correctly reproduced on the basis of a topological operation from the smallest elongated B_{10}^{2-} cluster.[14]

Fig. 3 illustrates the formation of the quasi-planar B_{56} structure following application of the leapfrog principle. Motivated by the presence of two hexagonal holes of B_{56} structure **A** (Fig. 1), a structure where a joint of two B_7 global minima geometries is selected as the starting point of the leapfrog process.

As shown in Fig. 3, the dual topological operation transforms the initial structure (**I**) in a new geometry formed by ten new hexagons surrounding the initial ones (**II**). The internal boron atoms of the initial hexagons of new geometry (**II**) are removed by the omni-capping [O] operation, whereas the other hexagons remain capped. The resulting geometry of this operation is a B_{48} planar geometry, namely the structure (**III**), being thus four times as large as the number of atoms of the parent geometry B_{12}. In the carbon derivatives, the latter structure obtained in such a way has empty corner spaces, but because the boron is electron deficient, these corners must be filled by additional atoms leading to structure (**IV**). Accordingly, eight extra atoms need to be added, and as a result a B_{56} structure (**V** and **VI**) can finally be established. It should be mentioned that the leapfrog operations can only lead to a strictly planar shape. The quasi-planar form of the most stable isomer **A** (Fig. 1) with a slight out-of-the-plan distortion comes from a full geometry optimization.

2.3 Electronic structure of the quasi-planar B_{56}

The shape of the most stable B_{56} isomer can thus be predicted by the topological leapfrog principle such as in the case of B_{50}. Therefore, it is expected that they share some similarities in their electronic structure as well as in a predominant property. According to a previous study, the high thermodynamic stability of the quasi-planar B_{50} was rationalized by using the disk aromaticity model involving the motion of a particle in a circular box.[14] In this context, the electronic structure of the quasi-planar B_{56}, particularly its π electrons, is now examined also using this model.

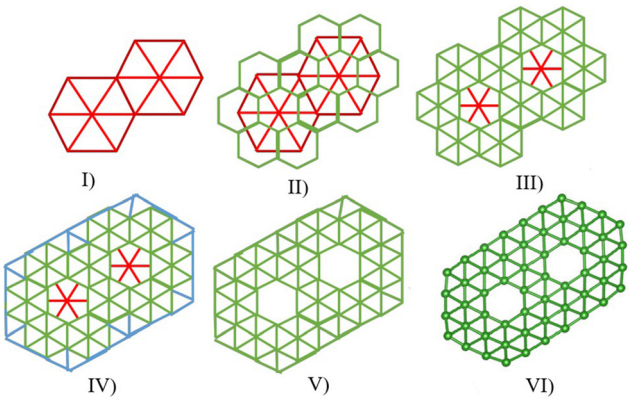

Fig. 3 A topological leapfrog operation applied to B_{12} leading to B_{56}: (**I**) B_{12} formed from two joint hexagons, (**II**) dual operation [O] and [D] applied to the B_{12}, (**III**) the resulting B_{48}, (**IV**) B-capping operation, and (**V**) and (**VI**) the resulting B_{56}.

The formalism of the model of a particle moving in a circular box has been given in much detail in previous studies.[13–15] Briefly, the eigenstates and eigenvalues of a circular disk depend on two quantum numbers including the principal number n and the rotational number l. The principal quantum number has value of 0, 1, 2, 3,... whereas the rotational number l has value 0, ±1, ±2, ±3, ±4, ±5, ±6,..., and the corresponding eigenstates are denoted as σ, π, δ, ϕ, γ, η, θ,.... The two values of a number l give rise to a degenerate state. Examination on electronic structure of the quasi-planar B_{56} **A** (Fig. 4) shows that its 19 π MOs are excellently produced by the model of a particle moving in a circular box.

Fig. 4 displays the 8 π-MOs of B_{56} including the LUMO. Accordingly, both LUMO and HOMO are associated with the 1θ level which is the degenerate eigenstates corresponding to the quantum numbers n = 1 and l = ±6. The HOMO−1 and HOMO−2 are well presented by the degenerate 2ϕ eigenstates involving the numbers n = 2 and l = ±4. On the basis of the point group irreducible representations of HOMO−4 and HOMO−6, they are associated with the 1η level of the model having quantum numbers n = 1 and l = ±5. The HOMO−9 and HOMO−5 of B_{56} correspond to the 2δ eigenstate of model with n = 2 and l = ±2. It should be noted that due to the presence of two hexagonal holes, the 1η and 2δ levels interchange with each other. Another interesting result is the occupancy of the 1θ molecular orbital where only one of the two degenerate orbitals is occupied; the origin of such a phenomenon is a breaking of the degeneracy due to the oval shape of the quasi-planar boron structure.

While the 2π levels with n = 2 and l = ±1 are associated with the HOMO−10, HOMO−13, the HOMO−15, HOMO−17 are represented by the 1γ levels having n = 1 and l = ±4. The HOMO−23 corresponds to the 2σ eigenstate of the model. The HOMO−25 and HOMO−26 are excellently reproduced by the 1φ eigenstates characterized by n = 1 and l = ±3. The HOMO−40, HOMO−41 are defined by the 1π state of the model with n = 1, l = ±1, whereas the HOMO−38, HOMO−36 are reproduced by the 1δ eigenstate having n = 1 and l = ±2. Finally, the 1σ eigenstate of the model with the non-degenerate quantum numbers n = 1 and l = 0 corresponds to the HOMO−43. The planar B_{56} **A** (Fig. 1) thus is characterized by an orbital configuration of $[(1\sigma)^2\ (1\pi)^4\ (1\delta)^4\ (1\varphi)^4\ (2\sigma)^2\ (1\gamma)^4\ (2\pi)^4\ (2\delta)^4\ (1\eta)^4\ (2\varphi)^4\ (1\theta)^2\ (1\theta)^0 \ldots]$ (Fig. 4) with an occupancy of 38 π-electrons. This result points out that formation of the delocalized MO pattern which obeys the model of particle moving in circular box, yields an enhanced thermodynamic stability for the quasi-planar B_{56} cluster.

Finally, we perform an AdNDP analysis for B_{56} to understand the nature of the σ bonds and it is shown in Fig. 5 with the 2, 3 and 4 center-2 electron bonds. For this purpose, we employ the Multiwfn package developed by Chen *et al.*[47] This method allows to analyze the localization of the bonds and it gives an idea of the aromaticity or antiaromaticity of the systems.[48–50] This has been employed in quasi planar and cage boron systems.[51,52] From the figure, we observe that the cluster contains some localized bonds, especially in the outer region of the B_{56} quasi-planar structure. This fact can be seen in the

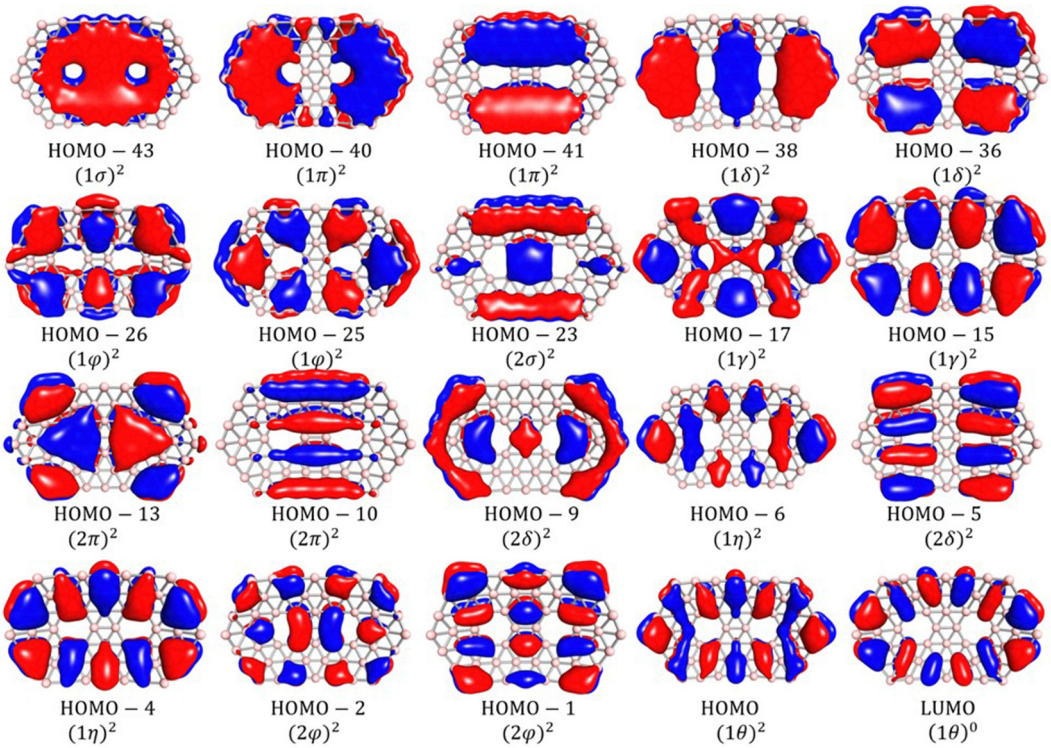

Fig. 4 Calculated π MOs (TPSSh/6-311+G(d)) of the quasi-planar B_{56} **A** (TPSSh/6-311+G(d)), their energy position levels with respect to the HOMO, and their assigned eigenstate (1σ, 1π, 1δ,...), according to the model of the a particle on moving in a circular box.

24 × |2c-2e| bonds in the external region of the cluster, while the two hexagons in the center of the cluster is surrounded by 12 bonds formed by 3-centers. Also, the system contains 29 × |4c-2e| bonds with 7 located in the inner region of the cluster and other 22 bonds in the outer region of the quasi-planar system. The remaining 19 bonds have a higher number of centers than 5; thus, these electrons are the π electrons that are part of the delocalized orbitals of the model described in the present study and previously suggested by Li *et al.*[53]

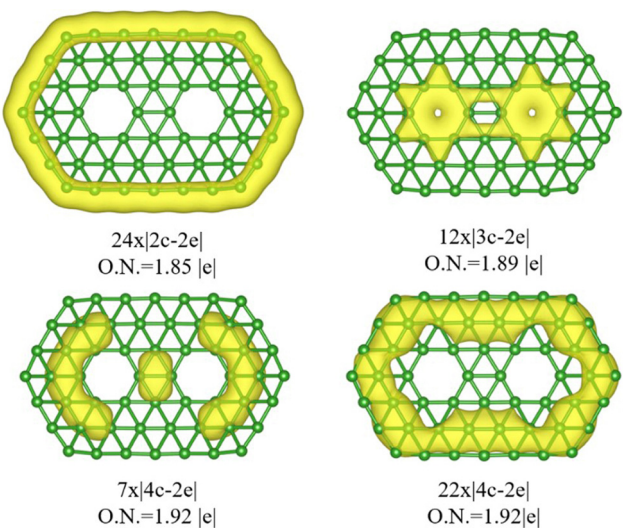

Fig. 5 An AdNDP analysis of the σ-orbitals of the most stable B_{56} isomer.

2.4 Magnetic current density in B_{56}

It has been known that the magnetic property of a species is related to its aromatic character. Calculations to obtain the magnetically perturbed density are performed using density functional theory with the PBE0 functional and the def2TZVP basis set using the gauge-including atomic orbitals. These calculations are performed using the Gaussian 16 program.[54] The magnetic current density ($\boldsymbol{J}(\boldsymbol{r})$) maps, and the delocalization index (DI) are calculated using the AIMALL program making using of the perturbed density.[55] The topology of the current density (tp$\boldsymbol{J}(\boldsymbol{r})$) and diatropicity ($C$) are numerically calculated with a set of python scripts that use the python library included in the Paraview 5.2.[56] The spacing in Cartesian grid used for the derivation and integration is 0.05 a.u. We previously showed that with such a spacing, the tp$\boldsymbol{J}(\boldsymbol{r})$ and C values smoothly converge.[57,58]

The tropicity of the magnetically induced current density ($\boldsymbol{J}(\boldsymbol{r})$) has often been used as a criterion for the aromaticity.[59–63] Accordingly, a diatropic current indicates an aromatic character whereas a paratropic current is related to an antiaromaticity. The main current at the cluster B_{56} is strongly paratropic (*cf.* Fig. 6(a)), contrary to that in the B_{50} which is a diatropic current.[14] The $\boldsymbol{J}(\boldsymbol{r})$ flux (defined as in the GIMIC method)[64] for both B_{50} and B_{56} clusters amount to −13.9 and 6.6 a.u., respectively. In this context, the paratropicity of the quasi-planar B_{56} **A** (Fig. 1) could wrongly suggest that it has a low thermodynamic stability due to its antiaromatic character. However, an explanation of the global paratropicity of B_{56} comes from the selection

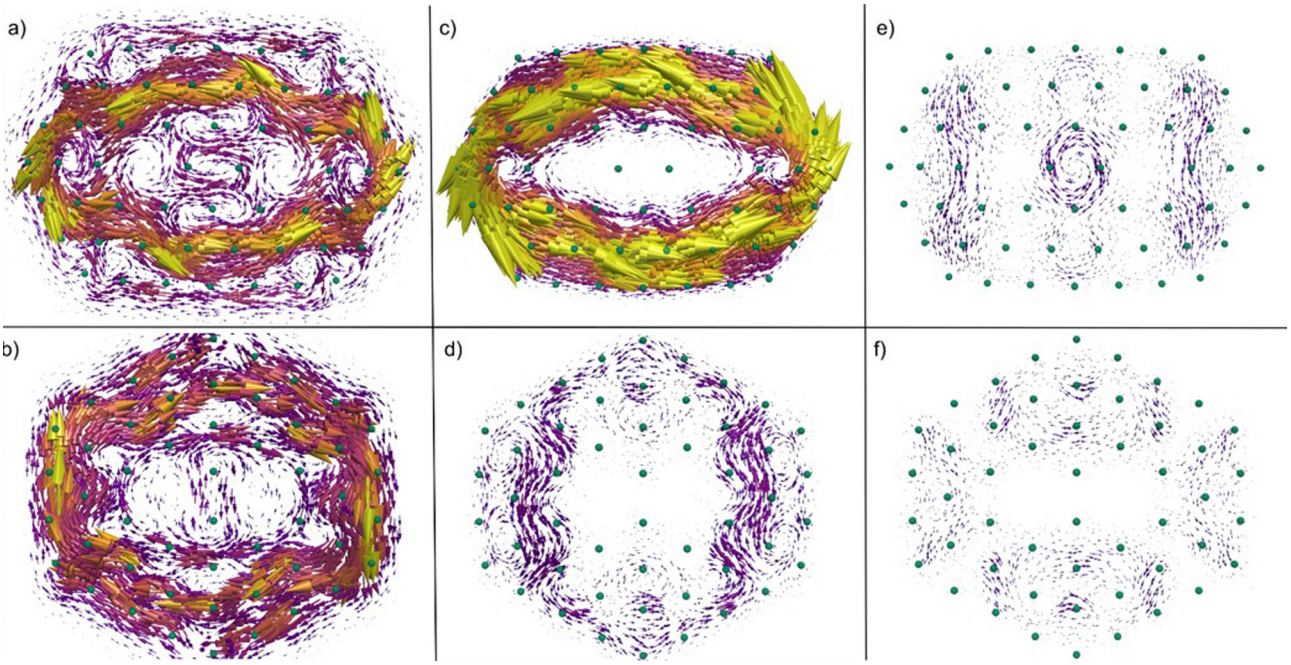

Fig. 6 $\boldsymbol{J}(\boldsymbol{r})$ vector maps of (a) B_{56}, (b) B_{50}, (c) B_{56}'s HOMO of B_{56}, (d) B_{50}'s HOMO of B_{50}, (e) B56's HOMO−1 of B_{56} and (f) B_{50}'s HOMO−1 of B_{50} at 1.0 bohr a.u. below the cluster. Color code: 0.00 a.u. blue, 0.75×10^{-3} a.u. purple and 1.5×10^{-3} a.u. Green dots are the positions of the boron atoms. Clockwise flows correspond to diatropic current densities.

rules involving the symmetry of its frontier orbitals. In fact, the global tropicity of a molecule is determined by the symmetry of its electronic transition, mainly from the HOMO to the LUMO.[65]

According to the known selection rules, the magnetic current is mainly paratropic when the product of the irreducible representations (Γ) of the orbitals involved in the electronic transition is rotationally allowed, whereas the current will be diatropic when this product is translationally allowed.[66] The intensity of the current depends on the energy gap between the occupied and unoccupied orbitals. In the case of the quasi-planar B_{56} **A**, the Γ product of its HOMO → LUMO transition is only rotationally allowed (A_2), whereas for the quasi-planar B_{50} this transition is both translationally and rotationally allowed (B_2). Moreover, the energy gap in B_{56} is smaller than that in B_{50} (30 *vs.* 42 kcal mol^{-1}, respectively). Fig. 6(c) shows that while the HOMO contribution to the current density is strongly paratropic for B_{56}, it is only slightly paratropic for B_{50} (Fig. 6(d)). This slightly paratropic current is compensated by diatropic currents of other orbitals, like the HOMO−1 (Fig. 6(f)). Overall, the quasi-planar B_{56} has a global paratropic current because the HOMO contribution is heavily paratropic due to the symmetry of the transition to the LUMO. This contribution cannot be compensated by transitions of other orbitals. On the other hand, the HOMO → LUMO transition on B_{50} is not associated with such a symmetry selection rule to generate a large paratropic $\boldsymbol{J}(\boldsymbol{r})$.

To further approach the question as to whether B_{56} is really anti-aromatic, let us consider another method to measure the tropicity of the current involved, which is actually the triple product of the current density (tp$\boldsymbol{J}(\boldsymbol{r})$) and the circulation ($C$).[57,58] Contrary to the flux of the magnetic ring current $\boldsymbol{J}(\boldsymbol{r})$, the tp$\boldsymbol{J}(\boldsymbol{r})$ maps of B_{56} and B_{50} turn out to be very similar to each other (*cf.* Fig. 7) in which both maps show strong diatropic and paratropic regions. The circulation (C) is diatropic for both B_{56} and B_{50} being −1.32 and −1.43 a.u., respectively. Moreover, these values are located in the low end of the corresponding values reported (from −1.4 to −3.5 a.u.) for a series of well-known polycyclic aromatic hydrocarbons (PAHs).[67] At a first glance, this result appears to be contradictory, because the flux of $\boldsymbol{J}(\boldsymbol{r})$ suggests a paratropicity for B_{56}, where the circulation (C) behaviour indicates a certain diatropicity. However, the flux and the C evaluate different properties. The term tp$\boldsymbol{J}(\boldsymbol{r})$ is defined as follows:

$$\mathrm{tp}\boldsymbol{J}(\boldsymbol{r}) = \mathbf{B}\cdot\nabla \times \boldsymbol{J}(\boldsymbol{r})$$

where $\mathbf{B}$ is the applied magnetic field and $\nabla \times \boldsymbol{J}(\boldsymbol{r})$ is the vorticity of the current density. The vorticity also allows us to define the circulation C which is the surface integral of $\nabla \times \boldsymbol{J}(\boldsymbol{r})$ divided by the surface area:

$$C = \frac{\int_s \nabla \times \boldsymbol{J}(\boldsymbol{r}) \cdot n\mathrm{d}s}{A_s}$$

The vorticity of $\boldsymbol{J}(\boldsymbol{r})$ is related to its local tropicity. Therefore, a tp$\boldsymbol{J}(\boldsymbol{r})$ map shows the local diatropic and paratropic regions and the C value is the sum of the tropicity of all local currents. For its part, the flux of $\boldsymbol{J}(\boldsymbol{r})$ mainly depends on the principal global current. Aihara *et al.* have already pointed out that $\boldsymbol{J}(\boldsymbol{r})$ patterns could not acquire the information on the local aromaticity and have shown in a series of small boron clusters that in some cases the global currents are paratropic, but the cluster is aromatic.[68–70] Accordingly, B_{50} can be regarded as both locally and globally diatropic whereas B_{56} is locally diatropic but globally paratropic. While the tropicity of $\boldsymbol{J}(\boldsymbol{r})$ does not seem

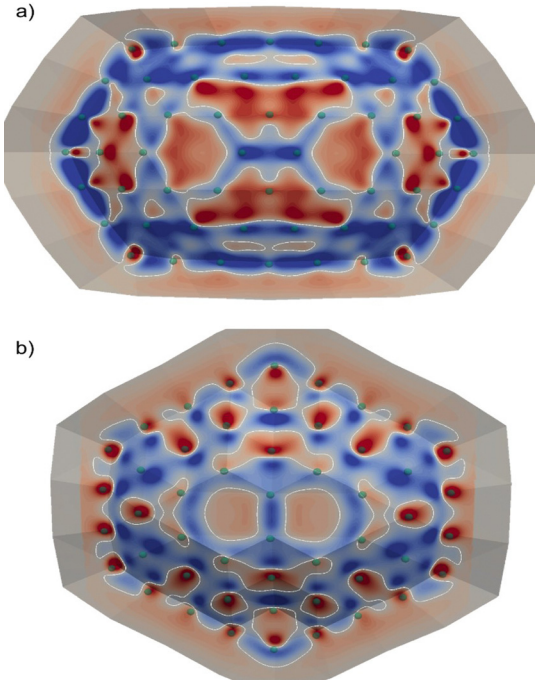

Fig. 7 tp$\boldsymbol{J}(\boldsymbol{r})$ of (a) B_{56} and (b) B_{50} at 1.0 bohr a.u. below under the cluster. Color code: $\leq -1.0 \times 10^{-3}$ a.u. dark blue, 0.0 a.u. white and $\geq 1.0 \times 10^{-3}$ a.u. A contour line (white) is drawn at 0.0 a.u. Negative values refer to diatropic regions.

to be conclusive with respect to the electron delocalization of B_{56}, the local tropicity coincides well with the high stability of the quasi-planar structure of B_{56}. These differences between both the local and global tropicities and its relationship with aromaticity deserve further studies on similar classes of clusters.

The delocalization index (DI) is also a useful parameter to evaluate the electron delocalization.[71,72] The DI is defined as follows:

$$\mathrm{DI} = \delta(A,B) = 2\left[\iint \left[\rho_2^{AB}(r_1,r_2) - \rho_A(r_1)\rho_B(r_2)\right] \mathrm{d}r_1 \mathrm{d}r_2\right]$$

where $\rho_2^{AB}(r_1,r_2)$ are called the matrix elements, while $\rho_A(r_1)$ and $\rho_B(r_2)$ are the density of each component.[73] The average values of the non-bonded DI values $\left(\left(\sum_i^N \mathrm{DI}_i^{\text{n-b}}\right)\Big/ N\right)$ are very similar for both the quasi-planar B_{50} and B_{56} species, namely 1.18×10^{-2} and 1.05×10^{-2} a.u., respectively. These values are in the same order of magnitude as in similar sizes of PAHs, namely the hexabenzocoronene $C_{42}H_{18}$ whose DI value amounts to 1.15×10^{-2} a.u.[64] Moreover, the DI values between two boron atoms at long distances are remarkably similar for both B_{50} and B_{56} (Table 1). Compared to the coronene $C_{42}H_{18}$, the boron cluster long-distance DIs are significantly larger than for the hydrocarbon compound, even though the B–B distances in B_{56} could significantly be longer than the C–C distances in $C_{42}H_{18}$. Poater *et al.* evaluated the DI values for the fullerene C_{60} and found that the DIs decay very rapidly with the distance.[74] The DI of the pair of carbons that are at opposite sides of the fullerene (with distance being 7.1 Å), is smaller than 5.0×10^{-4} a.u. Such a value is significantly lower than the DIs found for both B_{50} and B_{56} at significantly longer distances (*cf.* Table 1). This result indicates that the electrons of the boron clusters considered are more delocalized than those in hydrocarbon compounds of similar size. However, the DIs at three bonds distances within the hexagonal ring in both B_{56} and B_{50} are smaller than the values of the $C_{42}H_{18}$ (Table 1). The DI values of the boron clusters are also smaller than the value previously reported for C_{60} (4.6×10^{-2} a.u.).[74]

Table 1 Delocalization indices (DI) of both quasi-planar B_{56}, and B_{50} and hexabenzocoronene ($C_{42}H_{18}$). (see Fig. 8 for atom numbering)

Bond defined by atoms numbers	d (Å)	DI (10^{-2} a.u.)
B_{56}		
1–1″	14.186	0.359
7–6′	8.668	0.366
2_r–5_r	3.321	2.259
3_r–$3_r'$	3.350	3.176
B_{50}		
1–1″	11.137	0.084
6–7″	11.427	0.163
2_r–5_r	3.358	2.892
$C_{42}H_{18}$		
1–1″	11.301	0.090
2–2″	9.785	0.005
2–5	2.788	8.188[a]
2–6′	2.893	3.304[a]

[a] Values from ref. 57.

Taking together with the tp$\boldsymbol{J}(\boldsymbol{r})$ maps, these calculated results shows that contrary to the carbon-based compound in which the electrons are mainly delocalized within the individual benzene rings, the electrons in both quasi-planar B_{50} and

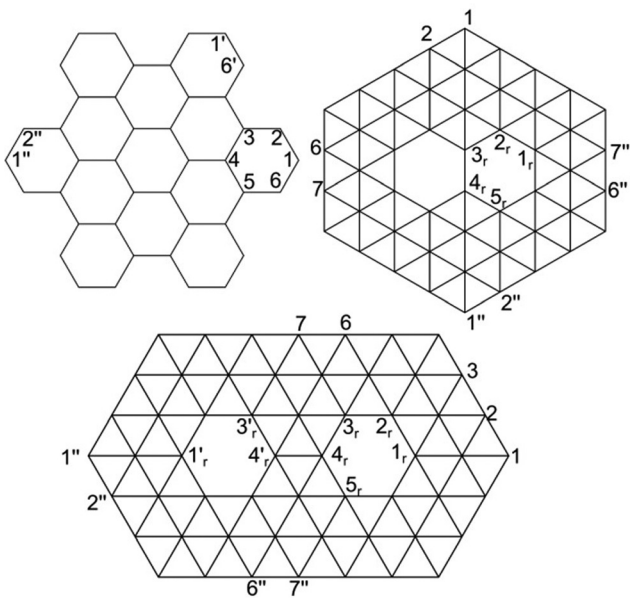

Fig. 8 Atom numbering for B_{50}, B_{56} and hexabenzocoronene $C_{42}H_{18}$ (*cf.* Table 1).

B_{56} clusters are delocalized across their whole molecular skeleton. The MO levels that can be reproduced by the particle in a circular box model, together with the DIs and the local tropicity (tp$\boldsymbol{J}(\boldsymbol{r})$ and C), suggest that the high thermodynamic stability of the quasi-planar B_{56} arises from a strong electron delocalization such as in the case of B_{50}.

3. Concluding remarks

In the present theoretical study, we demonstrated that the B_{56} cluster is stable in a quasi-planar form which contains two joint hexagonal holes. Such a structural motif can be predicted by using the topological leapfrog principle applied to a B_{12} unit. A significant step forward in understanding the geometrical shape of pure boron clusters has thus been made. Although it is a particular case, a piece of the mystery covering the growth pattern of the pure boron clusters comes out to light.

The high thermodynamic stability of the quasi-planar B_{56} structure is further rationalized in terms of the model of a particle moving in a circular disk and some other delocalization indices. The high thermodynamic stability of B_{56} comes from the strong π-electron delocalization, as in the case of the B_{50} cluster. The delocalization index DIs, the triple product of the current density tp$\boldsymbol{J}(\boldsymbol{r})$ and the circulation C values all show that the electrons are delocalized over the whole molecular skeleton and not in the hexagonal rings such as in some polyaromatic hydrocarbons. Such a conclusion is in agreement with the MOs whose shapes and locations can be rationalized by the particle in a circular box model, in which the π-electrons can move freely within the whole cluster.

It is interesting to note that the magnetic ring current flows of both quasi-planar B_{56} and B_{50} go in opposite directions, even though their electron delocalization patterns are similar. This behavior can be understood in considering the selection rule for the symmetry of the HOMO → LUMO electronic transition. In B_{50} this transition occurs in going from the 1η to the 2φ level which produces the expected diatropic current, whereas in B_{56} the same electronic transition occurs between the two 1θ levels which is only rotationally allowed and thereby produces a strong paratropic current. This is an addition to a few cases previously reported[64,73,74] in which a seemingly stable structure shows a magnetic paratropic current flow and points out the importance of the use of several electron delocalization indices in probing the aromaticity.

Conflicts of interest

The authors declare no competing financial interest.

Acknowledgements

The work of HTP and MTN is funded by VinGroup (Vietnam) and supported by VinGroup Innovation Foundation (VinIF) under project code VinIF.2020.DA21. The work of J. E. B.-L. is founded by DGAPA-UNAM (grant IN208820). MBS acknowledges the supercomputing center at UNAM for the use of their facilities. FBZ thanks Christian A. Celaya for his comments in the electronic analysis.

References

1 I. Boustani, *Molecular modelling and synthesis of nanomaterials: Applications in carbon-and boron-based nanotechnology*, Springer Nature, 2020, vol. 290.

2 H. R. Li, T. Jian, W. L. Li, C. Q. Miao, Y. J. Wang, Q. Chen, X. M. Luo, K. Wang, H. J. Zhai, S. D. Li and L. S. Wang, Competition between quasi-planar and cage-like structures in the B_{29}-cluster: Photoelectron spectroscopy and: *ab initio* calculations, *Phys. Chem. Chem. Phys.*, 2016, **18**(42), 29147–29155, DOI: **10.1039/c6cp05420j**.

3 T. B. Tai and M. T. Nguyen, Electronic structure and photoelectron spectra of B_n with n = 26–29: An overview of structural characteristics and growth mechanism of boron clusters, *Phys. Chem. Chem. Phys.*, 2015, **17**(20), 13672–13679, DOI: **10.1039/c5cp01851j**.

4 H. T. Pham, K. Z. Lim, R. W. A. A. Havenith and M. T. Nguyen, Aromatic character of planar boron-based clusters revisited by ring current calculations, *Phys. Chem. Chem. Phys.*, 2016, **18**(17), 11919–11931, DOI: **10.1039/c5cp07391j**.

5 T. B. Tai, L. Duong, H. T. Van Pham, D. T. T. Mai and M. T. Nguyen, A disk-aromatic bowl cluster B_{30}: Toward formation of boron buckyballs, *Chem. Commun.*, 2014, **50**(13), 1558–1560, DOI: **10.1039/C3CC48392D**.

6 T. B. Tai, R. W. A. Havenith, J. L. Teunissen, A. R. Dok, S. D. Hallaert, M. T. Nguyen and A. Ceulemans, Particle on a boron disk: Ring currents and disk aromaticity in B_{20}^{2-}, *Inorg. Chem.*, 2013, **52**(18), 10595–10600, DOI: **10.1021/ic401596s**.

7 H. T. Pham, L. v Duong, N. M. Tam, M. P. Pham-Ho and M. T. Nguyen, The boron conundrum: Bonding in the bowl B_{30} and B_{36}, fullerene B_{40} and triple ring B_{42} clusters, *Chem. Phys. Lett.*, 2014, **608**, 295–302, DOI: **10.1016/j.cplett.2014.05.069**.

8 L. Rincon, R. Almeida, J. E. Alvarellos, D. Garcia-Aldea, A. Hasmy and C. Gonzalez, The Σ delocalization in planar boron clusters, *J. Chem. Soc., Dalton Trans.*, 2009, 3328–3333, DOI: **10.1039/b818068g**.

9 P. Cias, M. Araki, A. Denisov and J. P. Maier, Gas phase detection of cyclic B_3: 22E′ ← X2A′1 electronic origin band, *J. Chem. Phys.*, 2004, **121**(14), 6776–6778, DOI: **10.1063/1.1791153**.

10 T. B. Tai, N. M. Tam and M. T. Nguyen, The boron conundrum: The case of cationic clusters Bn+ with n = 2–20, *Theor. Chem. Acc.*, 2012, **131**(6), 1–15, DOI: **10.1007/s00214-012-1241-8**.

11 R. Islas, D. Inostroza, D. Arias-Olivares, B. Zúñiga-Gutiérrez, J. Poater and M. Solà, Analysis of the electronic delocalization in some isoelectronic analogues of B_{12} doped with beryllium and/or carbon, *Phys. Chem. Chem. Phys.*, 2020, **22**(21), 12245–12259, DOI: **10.1039/d0cp01844a**.

12 X. M. Luo, T. Jian, L. J. Cheng, W. L. Li, Q. Chen, R. Li, H. J. Zhai, S. D. Li, A. I. Boldyrev, J. Li and L. S. Wang, B_{26}^{-}:

The Smallest planar boron cluster with a hexagonal vacancy and a complicated potential landscape, *Chem. Phys. Lett.*, 2017, **683**, 336–341, DOI: 10.1016/j.cplett.2016.12.051.
13 H. T. Pham, K. Z. Lim, R. W. A. Havenith and M. T. Nguyen, Aromatic character of planar boron-based clusters revisited by ring current calculations, *Phys. Chem. Chem. Phys.*, 2016, **18**(17), 11919–11931, DOI: 10.1039/c5cp07391j.
14 H. T. Pham, J. T. Muya, F. Buendía, A. Ceulemans and M. T. Nguyen, Formation of the quasi-planar B_{50} boron cluster: Topological path from B_{10} and disk aromaticity, *Phys. Chem. Chem. Phys.*, 2019, **21**(13), 7039–7044, DOI: 10.1039/c9cp00735k.
15 T. B. Tai, A. Ceulemans and M. T. Nguyen, Disk aromaticity of the planar and fluxional anionic boron clusters $B_{20}^{-/2-}$, *Chem. – Eur. J.*, 2012, **18**(15), 4510–4512, DOI: 10.1002/chem.201104064.
16 Z. A. Piazza, H.-S. Hu, W.-L. Li, Y.-F. Zhao, J. Li and L.-S. Wang, Planar hexagonal B_{36} as a potential basis for extended single-atom layer boron sheets, *Nat. Commun.*, 2014, **5**(1), 3113, DOI: 10.1038/ncomms4113.
17 Q. Chen, W. J. Tian, L. Y. Feng, H. G. Lu, Y. W. Mu, H. J. Zhai, S. D. Li and L. S. Wang, Planar B_{38}^- and B_{37}^- clusters with a double-hexagonal vacancy: Molecular motifs for borophenes, *Nanoscale*, 2017, **9**(13), 4550–4557, DOI: 10.1039/c7nr00641a.
18 Q. Chen, S.-Y. Zhang, H. Bai, W.-J. Tian, T. Gao, H.-R. Li, C.-Q. Miao, Y.-W. Mu, H.-G. Lu, H.-J. Zhai and S.-D. Li, Cage-LIke B_{41}^+ and B_{42}^{2+}: New chiral members of the borospherene family, *Angew. Chem., Int. Ed.*, 2015, **127**(28), 8278–8282, DOI: 10.1002/ange.201501588.
19 X. Y. Zhao, Q. Chen, H. R. Li, Y. W. Mu, H. G. Lu and S. D. Li, Cage-like B_{39}^+ clusters with the bonding pattern of $\sigma + \pi$ Double delocalization: New members of the borospherene family, *Phys. Chem. Chem. Phys.*, 2017, **19**(18), 10998–11003, DOI: 10.1039/c7cp00725f.
20 J. T. Muya, B. K. Isamura, I. Patouossa, M. T. Nguyen and A. Ceulemans, Structure, stability and bonding of the Leap-frog B_{240}, $\pm$ 1, $\pm$ 2, *J. Comput. Chem.*, 2021, **42**(2), 72–80, DOI: 10.1002/jcc.26434.
21 W. An, S. Bulusu, Y. Gao and X. C. Zeng, Relative stability of planar *versus* double-ring tubular isomers of neutral and anionic boron cluster B_{20} and B_{20}^-, *J. Chem. Phys.*, 2006, **124**(15), 154310, DOI: 10.1063/1.2187003.
22 W. L. Li, R. Pal, Z. A. Piazza, X. C. Zeng and L. S. Wang, B_{27}^-: Appearance of the smallest planar boron cluster containing a hexagonal vacancy, *J. Chem. Phys.*, 2015, **142**(20), 204305, DOI: 10.1063/1.4921732.
23 L. Cheng, B_{14}: An all-boron fullerene, *J. Chem. Phys.*, 2012, **136**(10), 104301, DOI: 10.1063/1.3692183.
24 T. Jian, X. Chen, S. D. Li, A. I. Boldyrev, J. Li and L. S. Wang, Probing the Structures and Bonding of Size-Selected Boron and Doped-Boron Clusters, *Chem. Soc. Rev.*, 2019, 3550–3591, DOI: 10.1039/c9cs00233b.
25 L. Duong, H. T. van; Pham, N. M. Tam and M. T. Nguyen, A particle on a hollow cylinder: The triple ring tubular cluster B_{27}^+, *Phys. Chem. Chem. Phys.*, 2014, **16**(36), 19470–19478, DOI: 10.1039/c4cp01996b.
26 Q. Chen, W. L. Li, X. Y. Zhao, H. R. Li, L. Y. Feng, H. J. Zhai, S. D. Li and L. S. Wang, B_{33}^- and B_{34}^-: Aromatic planar boron clusters with a hexagonal vacancy, *Eur. J. Inorg. Chem.*, 2017, 4546–4551, DOI: 10.1002/ejic.201700573.
27 W. L. Li, Q. Chen, W. J. Tian, H. Bai, Y. F. Zhao, H. S. Hu, J. Li, H. J. Zhai, S. D. Li and L. S. Wang, The B_{35} cluster with a double-hexagonal vacancy: A new and more flexible structural motif for borophene, *J. Am. Chem. Soc.*, 2014, **136**(35), 12257–12260, DOI: 10.1021/ja507235s.
28 X. Wu, X. Wu, X. Wu, L. Sai, S. Zhou, P. Zhou, M. Chen, M. Springborg and J. Zhao, Competition between tubular, planar and cage geometries: A complete picture of structural evolution of B: $N(n = 31–50)$ clusters, *Phys. Chem. Chem. Phys.*, 2020, **22**(23), 12959–12966, DOI: 10.1039/d0cp01256d.
29 T. B. Tai and M. T. Nguyen, A new chiral boron cluster B_{44} containing nonagonal holes, *Chem. Commun.*, 2016, **52**(8), 1653–1656, DOI: 10.1039/c5cc09111j.
30 L. Sai, X. Wu, N. Gao, J. Zhao and R. B. King, Boron clusters with 46, 48, and 50 atoms: Competition among the core–shell, bilayer and quasi-planar structures, *Nanoscale*, 2017, **9**(37), 13905–13909, DOI: 10.1039/c7nr02399e.
31 Q. Q. Yan, L. Pei and S. D. Li, Predicting bilayer B_{50}, B_{52}, B_{56}, and B_{58}: Structural evolution in bilayer B_{48}–B_{72} clusters, *J. Mol. Model.*, 2021, **27**(12), 364, DOI: 10.1007/s00894-021-04954-3.
32 L. Pei, Y. Y. Ma, M. Yan, M. Zhang, R. N. Yuan, Q. Chen, W. Y. Zan, Y. W. Mu and S. D. Li, Bilayer B_{54}, B_{60}, and B_{62} clusters in a universal structural pattern, *Eur. J. Inorg. Chem.*, 2020, 3296–3301, DOI: 10.1002/ejic.202000473.
33 W. J. Chen, Y. Y. Ma, T. T. Chen, M. Z. Ao, D. F. Yuan, Q. Chen, X. X. Tian, Y. W. Mu, S. D. Li and L. S. Wang, B_{48}^-: A bilayer boron cluster, *Nanoscale*, 2021, **13**(6), 3868–3876, DOI: 10.1039/d0nr09214b.
34 B. K. Rao and P. Jena, Evolution of the electronic structure and properties of neutral and charged aluminum clusters: A comprehensive analysis, *J. Chem. Phys.*, 1999, **111**(5), 1890–1904, DOI: 10.1063/1.479458.
35 A. Aguado and J. M. López, Structures and stabilities of Aln+, Aln, and Aln− (N = 13–34) clusters, *J. Chem. Phys.*, 2009, **130**(6), 064704, DOI: 10.1063/1.3075834.
36 N. Drebov and R. Ahlrichs, Structures of Aln, its anions and cations up to N = 34: A theoretical investigation, *J. Chem. Phys.*, 2010, **132**(16), 164703, DOI: 10.1063/1.3403692.
37 C. Li, W. Tang and V. Vahabi, Identification of sulfur gases by an B_{40} fullerene: A computational study, *Phys. E*, 2020, **120**, 1–8, DOI: 10.1016/j.physe.2020.114038.
38 X. Sun, K. Wang, P. Yin, Y. Zhang and X. Feng, Quasi-planar B_{50} sheet as a potential molecular sensor for NO_2: A DFT study, *Mater. Chem. Phys.*, 2021, **260**, 1–7, DOI: 10.1016/j.matchemphys.2020.124104.
39 J. A. Vargas, F. Buendía and M. R. Beltrán, New AuN (N = 27–30) lowest energy clusters obtained by means of an improved DFT-genetic algorithm methodology, *J. Phys. Chem. C*, 2017, **121**(20), 10982–10991, DOI: 10.1021/acs.jpcc.6b12848.
40 G. Kresse, Ab Initio Molecular-Dynamics Simulation of the Liquid-Metal-Amorphous-Semiconductor Transition in Germanium, *Phys. Rev. B: Condens. Matter Mater. Phys.*, 1994, **8**, 14251–14269.

41 G. Kresse and J. Furthmuller, Efficient iterative schemes for *ab initio* total-energy calculations using a plane-wave basis set, *Phys. Rev. B: Condens. Matter Mater. Phys.*, 1996, **54**, 11169–11186.

42 G. Kresse and J. Hafner, Ab Initio Molecular Dynamics For Liquid Metals, *Phys. Rev. B: Condens. Matter Mater. Phys.*, 1993, **47**, 558–561.

43 G. Kresse and J. Furthmuller, Efficiency of *ab initio* total energy calculations for metals and semiconductors using a plane-wave basis set, *Comput. Mater. Sci.*, 1996, **6**, 15–50.

44 J. P. Perdew, K. Burke and Y. Wang, Generalized gradient approximation for the exchange-correlation hole of a many-electron system, *Phys. Rev. B: Condens. Matter Mater. Phys.*, 1996, **54**, 16533–16539.

45 J. Zhao, L. Wang, F. Li and Z. Chen, B_{80} and other medium-sized boron clusters: Core–shell structures, not hollow cages, *J. Phys. Chem. A*, 2010, **114**(37), 9969–9972, DOI: **10.1021/jp1018873**.

46 P. W. Fowler and J. I. Steer, The Leapfrog principle: A rule for electron counts of carbon clusters, *J. Chem. Soc., Chem. Commun.*, 1987, 1403–1405.

47 T. Lu and F. Chen, Multiwfn: A multifunctional wavefunction analyzer, *J. Comput. Chem.*, 2012, **33**(5), 580–592, DOI: **10.1002/jcc.22885**.

48 D. Yu Zubarev and A. I. Boldyrev, Deciphering chemical bonding in golden cages, *J. Phys. Chem. A*, 2009, **113**(5), 866–868, DOI: **10.1021/jp808103t**.

49 D. Yu Zubarev and A. I. Boldyrev, Developing paradigms of chemical bonding: Adaptive natural density partitioning, *Phys. Chem. Chem. Phys.*, 2008, **10**(34), 5207–5217, DOI: **10.1039/B804083D**.

50 D. Yu Zubarev and A. I. Boldyrev, Revealing intuitively assessable chemical bonding patterns in organic aromatic molecules *via* adaptive natural density partitioning, *J. Org. Chem.*, 2008, **73**(23), 9251–9258, DOI: **10.1021/jo801407e**.

51 O. A. Gapurenko, R. M. Minyaev, N. S. Fedik, V. v Koval, A. I. Boldyrev and V. I. Minkin, Structure and bonding of new boron and carbon superpolyhedra, *Struct. Chem.*, 2019, **30**(3), 805–814, DOI: **10.1007/s11224-019-1279-5**.

52 I. Patouossa, A. G. Arvanitidis, J. Tshishimbi Muya, M. T. Nguyen and A. Ceulemans, Valence bonds in planar and quasi-planar boron disks, *Phys. Chem. Chem. Phys.*, 2019, **21**(2), 729–735, DOI: **10.1039/c8cp06749j**.

53 W. J. Tian, Q. Chen, X. X. Tian, Y. W. Mu, H. G. Lu and S. D. Li, From Quasi-Planar B_{56} to penta-ring tubular Ca©B_{56}: Prediction of metal-stabilized Ca©B_{56} as the embryo of metal-doped boron α-nanotubes, *Sci. Rep.*, 2016, **6**, 37893, DOI: **10.1038/srep37893**.

54 M. J. Frisch, G. W. Trucks, H. B. Schlegel, G. E. Scuseria, M. A. Robb, J. R. Cheeseman, G. Scalmani, V. Barone, G. A. Petersson, H. Nakatsuji, X. Li, M. Caricato, A. v Marenich, J. Bloino, B. G. Janesko, R. Gomperts, B. Mennucci, H. P. Hratchian, J. v Ortiz, A. F. Izmaylov; J. L. Sonnenberg, D. Williams-Young, F. Ding, F. Lipparini, F. Egidi, J. Goings, B. Peng, A. Petrone, T. Henderson, D. Ranasinghe, V. G. Zakrzewski, J. Gao, N. Rega, G. Zheng, W. Liang, M. Hada, M. Ehara, K. Toyota, R. Fukuda, J. Hasegawa, M. Ishida, T. Nakajima, Y. Honda, O. Kitao, H. Nakai, T. Vreven, K. Throssell, J. A. Montgomery Jr., J. E. Peralta, F. Ogliaro, M. J. Bearpark, J. J. Heyd, E. N. Brothers, K. N. Kudin, V. N. Staroverov, T. A. Keith, R. Kobayashi, J. Normand, K. Raghavachari, A. P. Rendell, J. C. Burant, S. S. Iyengar, J. Tomasi, M. Cossi, J. M. Millam, M. Klene, C. Adamo, R. Cammi, J. W. Ochterski, R. L. Martin, K. Morokuma, O. Farkas, J. B. Foresman and D. J. Fox, *Gaussian 16 Revision C.01.*, 2016.

55 AIMAll (Version 19.10.12), Todd A. Keith, TK Gristmill Software, Overland Park KS, USA, 2019 (Aim.Tkgristmill.Com). AIMAll (Version 19.10.12), Todd A. Keith, TK Gristmill Software, Overland Park KS, USA, 2019 (aim.tkgristmill.com). 2019.

56 J. Ahrens; B. Geveci and C. Law, Paraview: An end-user tool for large data visualization, *Visualization Handbook*, Elsevier, 2005.

57 J. E. Barquera-Lozada, Vorticity: Simplifying the analysis of the current density, *J. Comput. Chem.*, 2019, **40**(30), 2602–2610, DOI: **10.1002/jcc.26018**.

58 J. E. Barquera-Lozada, The vorticity of the current density tensor and 3D-aromaticity, *Int. J. Quantum Chem.*, 2019, **119**(8), 1–12, DOI: **10.1002/qua.25848**.

59 D. Sundholm, H. Fliegl and R. J. F. Berger, Calculations of magnetically induced current densities: Theory and applications, *Wiley Interdiscip. Rev.: Comput. Mol. Sci.*, 2016, **6**(6), 639–678, DOI: **10.1002/wcms.1270**.

60 R. Gershoni-Poranne and A. Stanger, Magnetic criteria of aromaticity, *Chem. Soc. Rev.*, 2015, 6597–6615, DOI: **10.1039/c5cs00114e**.

61 A. Kumar, M. Duran and M. Solà, Is coronene better described by Clar's aromatic π-sextet model or by the AdNDP representation?, *J. Comput. Chem.*, 2017, **38**(18), 1606–1611, DOI: **10.1002/jcc.24801**.

62 G. Monaco, L. T. Scott and R. Zanasi, Magnetic euripi in corannulene, *J. Phys. Chem. A*, 2008, **112**(35), 8136–8147, DOI: **10.1021/jp8038779**.

63 R. Báez-Grez, W. A. Rabanal-León, L. Alvarez-Thon, L. Ruiz, W. Tiznado and R. Pino-Rios, Aromaticity in heterocyclic analogues of benzene: Dissected nics and current density analysis, *J. Phys. Org. Chem.*, 2019, **32**(1), 1–7, DOI: **10.1002/poc.3823**.

64 J. Jusélius, D. Sundholm and J. Gauss, Calculation of current densities using gauge-including atomic orbitals, *J. Chem. Phys.*, 2004, **121**(9), 3952–3963, DOI: **10.1063/1.1773136**.

65 G. Monaco, M. Memoli and R. Zanasi, Additivity of current density patterns in altan-molecules, *J. Phys. Org. Chem.*, 2013, **26**(2), 109–114, DOI: **10.1002/poc.2958**.

66 M. K. Cyrański, R. W. A. Havenith, M. A. Dobrowolski, B. R. Gray, T. M. Krygowski, P. W. Fowler and L. W. Jenneskens, The phenalenyl motif: A magnetic chameleon, *Chem. – Eur. J.*, 2007, **13**(8), 2201–2207, DOI: **10.1002/chem.200601619**.

67 E. M. Rico-Sotomayor and J. E. Barquera-Lozada, Triangulenes and theirs ions: Reaching the limits of Clar's rule, *Phys. Chem. Chem. Phys.*, 2020, **22**(42), 24704–24711, DOI: **10.1039/d0cp03305g**.

68 J. Aihara and S. Oe, Graph-theoretical Re-interpretation of NICS values for polycyclic aromatic hydrocarbons: Naphthalene and azulene, *Bull. Chem. Soc. Jpn.*, 2003, **76**(7), 1363–1364, DOI: **10.1246/bcsj.76.1363**.

69 J. Aihara, H. Kanno and T. Ishida, Aromaticity of planar boron clusters confirmed, *J. Am. Chem. Soc.*, 2005, **127**(38), 13324–13330, DOI: **10.1021/ja053171i**.

70 J. Aihara, Magnetic resonance energy and topological resonance energy, *Phys. Chem. Chem. Phys.*, 2016, **18**(17), 11847–11857, DOI: **10.1039/C5CP06471F**.

71 Y.-G. Wang and N. H. Werstiuk, A Practical and efficient method to calculate aim localization and delocalization indices at post-HF levels of theory, *J. Comput. Chem.*, 2003, **24**, 379–385.

72 R. F. W Bader and M. E. Stephens, Spatial localization of the electronic pair and number distributions in molecules, *J. Am. Chem. Soc.*, 1975, **97**, 7391–7399.

73 A. Martín Pendás, M. A. Blanco and E. Francisco, Chemical fragments in real space: Definitions, properties, and energetic decompositions, *J. Comput. Chem.*, 2007, **28**(1), 161–184, DOI: **10.1002/jcc.20469**.

74 J. Poater, M. Duran and M. Solà, Analysis of electronic delocalization in buckminsterfullerene (C 60), *Int. J. Quantum Chem.*, 2004, **98**(4), 361–366, DOI: **10.1002/qua.20071**.

